KSME

Springer

Journal of Mechanical Science and Technology 35 (8) 2021

Original Article
DOI 10.1007/s12206-021-0723-9

Keywords:
· Composite
· Hydrogen pressure vessel (type 4)
· Isotensoid
· Netting theory

Correspondence to:
Chul Kim
chulki@pusan.ac.kr

Citation:
Park, G., Jang, H., Kim, C. (2021). Design of composite layer and liner for structure safety of hydrogen pressure vessel (type 4). Journal of Mechanical Science and Technology 35 (8) (2021) 3507~3517.
http://doi.org/10.1007/s12206-021-0723-9

Received January 13th, 2021
Revised April 9th, 2021
Accepted May 4th, 2021

† Recommended by Editor
Hyun-Gyu Kim

Design of composite layer and liner for structure safety of hydrogen pressure vessel (type 4)

Gunyoung Park, Hyoseong Jang and Chul Kim

School of Mechanical Engineering, Pusan National University, Busan 46241, Korea

Abstract Due to the problems of fossil fuel exhaustion and environmental pollution, the use of hydrogen fuel has been increasing gradually, so there is also need of commercialization of hydrogen fuel cell vehicle. In order to increase its fuel efficiency, light-weightning and structural design, which are to optimize thickness and shape of the pressure vessel (end closure and boss) and winding angle of composite, have been required. This study has carried out as follows to obtain structural safety of hydrogen pressure vessel (type 4) under working pressure (700 bar). Plastic liner was designed using dome shape with isotensoid curve and spherical shape not to slip in the dome region while filament winding. After calculating the initial thickness of composite by netting theory, the composite thickness in both cylinder and dome parts to satisfy structural safety were obtained by FEM, changing the thicknesses calculated from theory. Also, optimal design of aluminium boss shape was performed using the response surface method to achieve light-weightning and increase of inner capacity. Based on the above results, structural safety of the optimal hydrogen pressure vessel (type 4) with the composite layer and boss shape finally determined was verified through FEA.

1. Introduction

The emissions from the use of fossil fuels have caused harmful substances, which threaten human health and the earth's environment, so there is an increase in the demand for clean and safe energy, and renewable energy is needed to be used to achieve sustainable energy systems [1, 2]. Especially in the public transport necessary for people's lives, hydrogen storage pressure vessel is one of important devices for new energy vehicles. As the air pollution becomes more serious, safe and lightweight energy storage pressure vessel is inevitable requirements for development of the automotive industry. There are four types of pressure vessel as shown Fig. 1, and their brief description is as follows [3, 4]:

Type 1 : Steel or aluminium alloy metal structure. The load is entirely borne by the metal.

Type 2 : Steel or aluminium liner. The cylinder part is made of a hoop wound long fiber reinforced composite pressure vessel. The load is shared by metal and composite.

Type 3 : Metal liner (typically aluminium) with full composite overwrap. Composite materials carry structural loads.

Type 4 : Non-metal liner (plastic liner). A carbon fiber composite is filament wound over a thermoplastic liner, and composite carries structural loads.

In the previous studies relating to composite pressure vessel, Ramirez presented the results of burst simulations performed on a pressure vessel (type 4) using commercial software ABAQUS [5]. Hayato studied the new design that has notch and optimized dome shape about the CFRP cryogenic tank, it can reduce energy release rate near the cap and prevent crack propagation [6]. Cho carried out a series of the hydraulic burst tests and the structural analyses for the composite cylinders (type 4) with different dome curvatures [7]. Alcantar proposed the use of genetic algorithm (GA) and simulated annealing (SA) using the Microsoft Visual Studio Tool Wintempla to optimize the composite weight of two pressure vessels (type 4) [8]. Roh

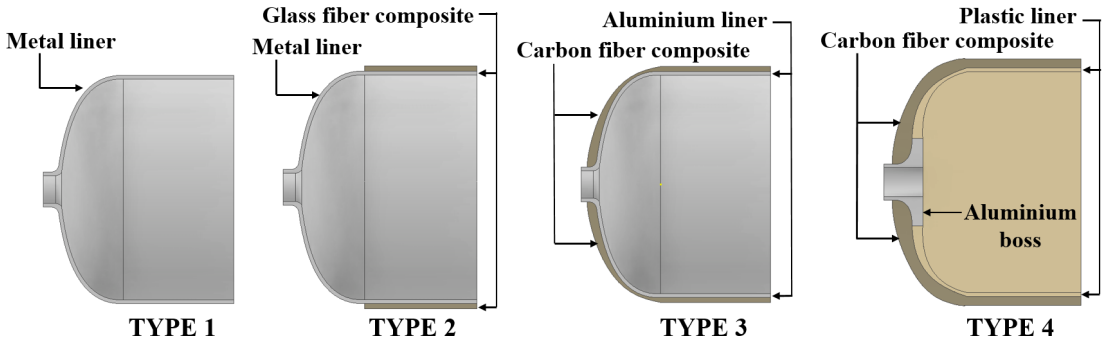

Fig. 1. Four types of pressure vessel.

identified the most vulnerable failure points in a 700-bar H2 storage tank (type 4) and proposed methods to reinforce the tank using a reduced amount of carbon fiber as compared to conventional filament winding techniques [9]. Hua studied on reducing the composite weight with modeling assessment of conventional tanks without doilies that utilize lower cost resin that also has a low density [10]. Leh presented and qualified an FE model taking into account progressive damage of the composite structure manufactured by filament winding and designed for a new optimization procedure developed specifically [11]. Lei studied the optimal shapes and fiber architectures of non-geodesics-based domes for pressure vessels upon the condition of equal shell strains [12]. Barboza performed burst pressure testing of LLDPE/HDPE liner, on both small-scale and full-scale, and the results of maximum hydrostatic pressure were compared to the ASME Boiler and Pressure Vessel Code, Sec. VIII, Division dimensioning procedure. And FEA was used to predict the vessel mechanical behavior [13]. Considering the previous studies, which were focused on shape of dome part and design and fracture of composite part for hydrogen pressure vessel (type 4), optimal design of it including shape of aluminium boss part to install valve for rechanging and supplying hydrogen, is needed.

This study has carried out design of pressure vessel (type 4) as shown Fig. 2 to obtain structural safety under working pressure (700 bar). The shape of plastic liner was designed using dome shape with isotensoid-spherical curves not to slip in the dome region while filament winding. And after calculating the initial thickness of composite by netting theory, the composite thickness in both cylinder and dome parts to satisfy structural safety were obtained by FEM, changing the thicknesses calculated from theory. Also, optimal design of aluminium boss shape was performed using the response surface method to achieve light-weightning and increase of inner capacity. Based on the above results, structural safety of the optimal pressure vessel (type 4) with the composite layer and the boss shape finally determined was verified through FEA.

2. Design of pressure vessel (type 4)

2.1 Design of isotensoid dome

Isotensoid dome is the most stable shape for filament wound composite pressure vessel, and it provides the dome structure with the minimum weight and maximum carrying capacity [14]. Dome shape of pressure vessel is rotated by a meridian axis, so equation for the meridian is needed to be established to obtain dome shell. A point (P) and a micro-element (ds) on the meridian line are illustrated in Fig. 3. 'r' is radius of the parallel circle from z-axis to 'P', and 'O' is center point of isotensoid curve. 'r_1' is the meridian curvature radius, and 'r_2' is circumferential curvature radius. 'r_c' and 'r_o' are radii of cylinder and boss, respectively, and 'φ' is angle between r_2 and z-axis.

The geometric relationship between r_1 and r_2 is expressed as Eq. (1).

$$\frac{r_2}{r_1}=\frac{r\cdot\cot\varphi\cdot d\varphi}{dr}. \tag{1}$$

According to the membrane shell theory shown in Fig. 4, circumferential line load (N_θ) and meridian line load (N_φ) subjected to internal pressure (P) are calculated by Eqs. (2) and (3), and the static equilibrium equation of the rotating shell is written as Eq. (4) [15].

$$N_\theta=\frac{1}{2}r_2p\left(2-\frac{r_2}{r_1}\right), \tag{2}$$

$$N_\varphi=\frac{1}{2}r_2p, \tag{3}$$

$$\frac{N_\varphi}{N_\theta}=2-\frac{r_2}{r_1}. \tag{4}$$

Based on the netting theory, circumferential line load (N_θ) and meridian line load (N_φ) on the dome part are calculated by Eqs. (5) and (6) as shown in Fig. 5 [16], and the relationship between N_θ and N_φ is expressed as Eq. (7). Where 'α' is laminated angle wound along a geodesic specified by the Clairaut shown in Eq. (8), without slippage on the dome part during the filament winding process, and σ_f is a longitudinal tensile strength of composite.

$$N_\theta=\sigma_f\cdot t\cdot\sin^2\alpha, \tag{5}$$

$$N_\varphi=\sigma_f\cdot t\cdot\cos^2\alpha, \tag{6}$$

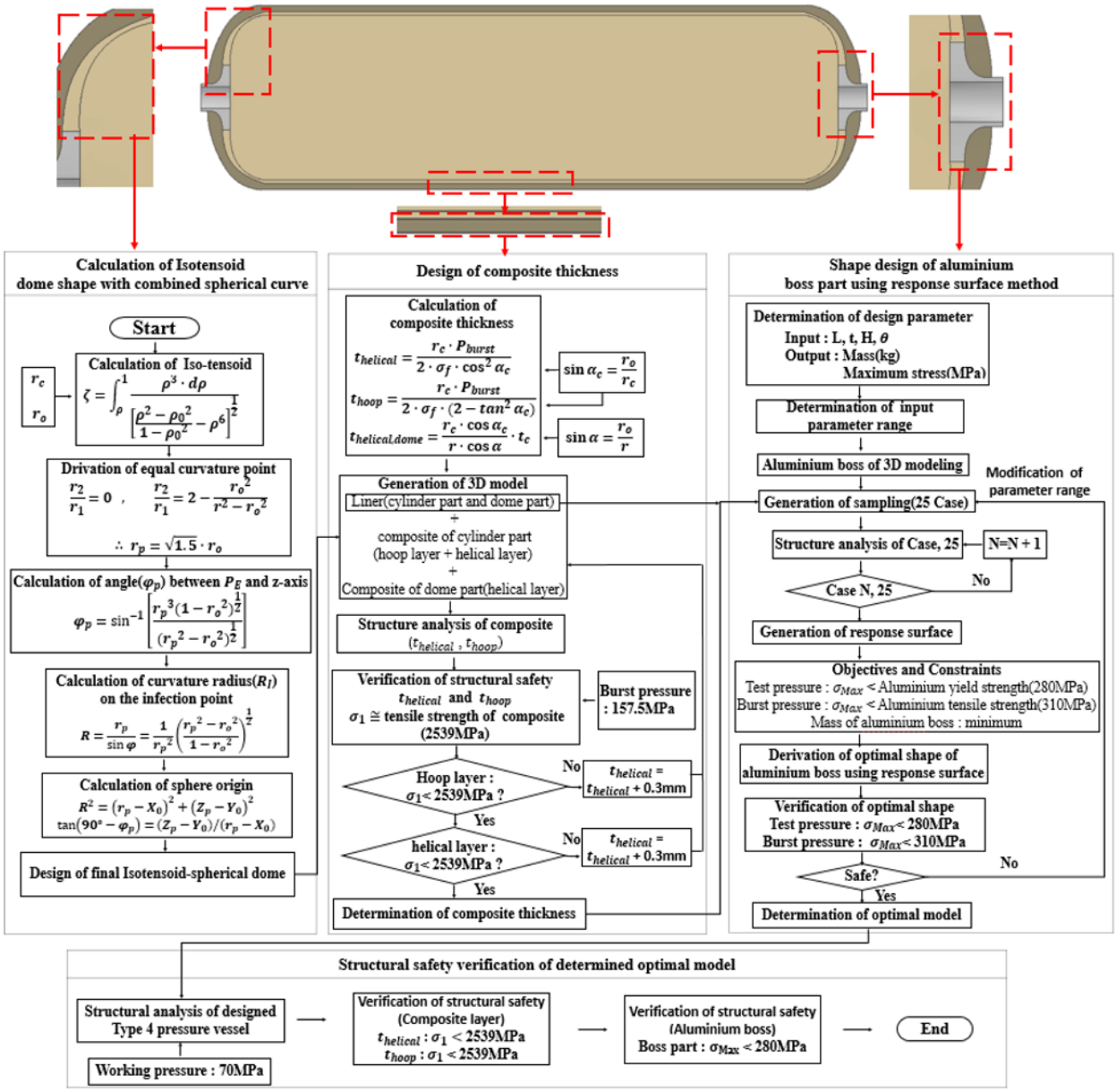

Fig. 2. Flow chart of optimum design of pressure vessel (type 4).

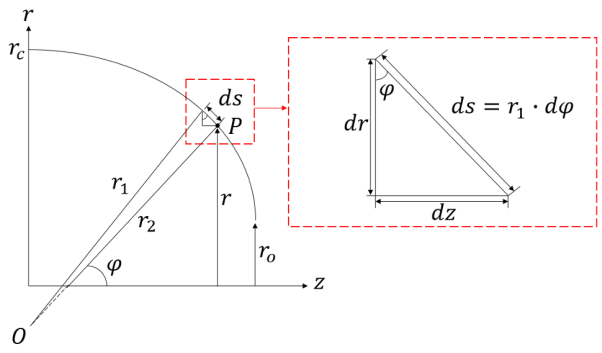

Fig. 3. Shell of revolution of isotensoid curve.

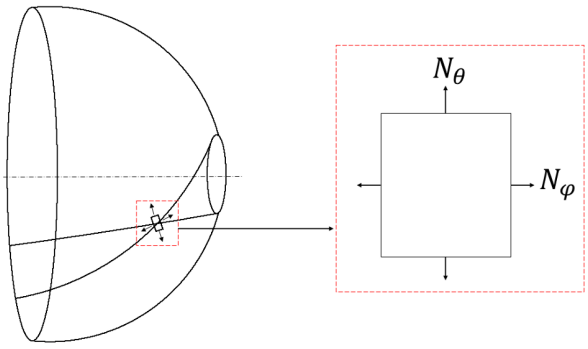

Fig. 4. Loads in membrane shell.

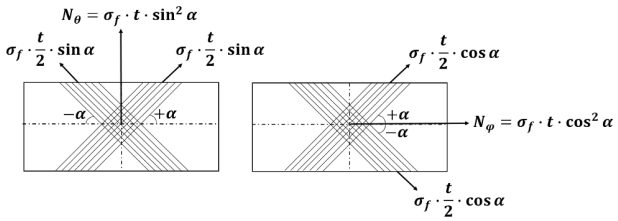

Fig. 5. Free-body diagram of oriented fibers in θ and φ directions.

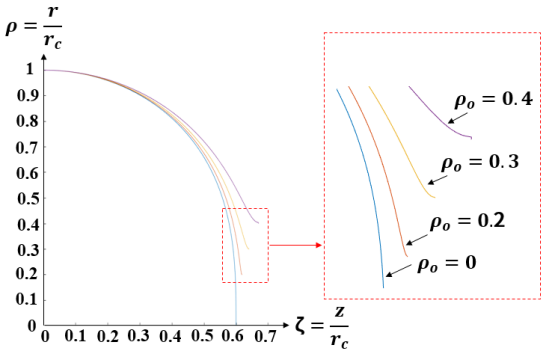

Fig. 6. Iso-tensoid curves with different ρ_0 and inflection points.

$$\frac{N_\theta}{N_\varphi} = \frac{\sin^2\alpha}{1-\sin^2\alpha}, \tag{7}$$

$$\sin\alpha = \frac{r_o}{r}. \tag{8}$$

From Eqs. (4), (7) and (8), the mechanical relationship between 'r_1' and 'r_2' is rewritten by Eq. (9)

$$\frac{r_2}{r_1} = 2 - \frac{r_o^2}{r^2 - r_o^2}. \tag{9}$$

2.2 Design of dome with combined isotensoid-spherical curve

Isotensoid curve is denoted as Eq. (10) from Eqs. (1) and (9) where, $\zeta = z/r_c$, $\rho = r/r_c$, and $\rho_o = r_o/r_c$ [14, 15].

$$\zeta = \int_\rho^1 \frac{\rho^3 d\rho}{\left[\frac{\rho^2 - \rho_0^2}{1-\rho_0^2} - \rho^6\right]^{\frac{1}{2}}}. \tag{10}$$

Isotensoid dome shapes by varying 'ρ_o' (= 0, 0.2, 0.3 and 0.4) were obtained using Eq. (10), and inflection points were observed at the ends of the isotensoid curves as shown in Fig. 6. Therefore, a part of the isotensoid curve with inflection point is needed to be removed, and then its substitute curve should be combined with the remaining isotensoid curve.

This study adopted spherical curve, and curvature radius (R) of shpere at a point (P_I) on the isotensoid dome, and angle (φ_p) between $\overline{O_{sphere}p}$ and z-axis, origin coordinate of the sphere, O_{sphere} (x_0, y_0) is calculated by using Eqs. (11)-(14) as shown Fig. 7.

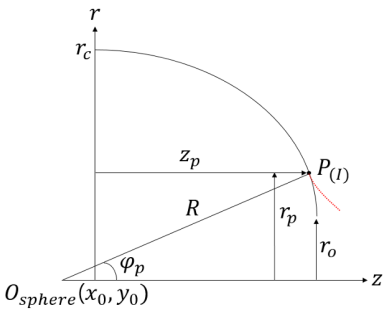

Fig. 7. Isotensoid curve combined with spherical curve.

$$R = \frac{r_p}{\sin\varphi} = \frac{1}{r_p^2}\left(\frac{r_p^2 - r_o^2}{1-r_o^2}\right)^{\frac{1}{2}}, \tag{11}$$

$$\varphi_p = \sin^{-1}\left[\frac{r_p^3\left(1-r_o^2\right)^{\frac{1}{2}}}{\left(r_p^2 - r_o^2\right)^{\frac{1}{2}}}\right], \tag{12}$$

$$R^2 = \left(r_p - y_0\right)^2 + \left(z_p - x_0\right)^2, \tag{13}$$

$$\tan\left(90° - \varphi_p\right) = \frac{z_p - x_0}{r_p - y_0}. \tag{14}$$

2.3 Design of composite layer

The cylindrical section of pressure vessel (type 4) is reinforced with helical and hoop windings, while only helical winding extends to the vessel head. Netting analysis through Eq. (15), which assumes that all loads are to be carried exclusively by the fiber with no assistance from the resin, is used to estimate the thicknesses of the helical and hoop layers in the cylindrical part [17]. Where, r_c : radius of cylinder, P_{burst} : burst pressure, σ_f : longitudinal I tensile strength, and $\alpha_c(r = r_c)$: helical angle of cylinder part, which is calculated by Eq. (8).

$$\begin{cases} t_{helical} = \dfrac{r_c \cdot P_{burst}}{2 \cdot \sigma_f \cdot \cos^2\alpha_c} \\ t_{hoop} = \dfrac{r_c \cdot P_{burst}}{2 \cdot \sigma_f \cdot \left(2 - \tan^2\alpha_c\right)} \end{cases}. \tag{15}$$

The thickness of composite layer in dome part is varied according to the dome radius, because the number of fiber aggregates on all cross-sections of the dome is the same as shown in Fig. 8. The thickness of helical layer in dome part is expressed as Eq. (16) [18, 19], where, 'α' means laminated angle of helical layer not slipping during filament winding according to variations of dome radius.

$$t = \frac{r_c \cdot \cos\alpha_c}{r \cdot \cos\alpha} \cdot t_{helical}. \tag{16}$$

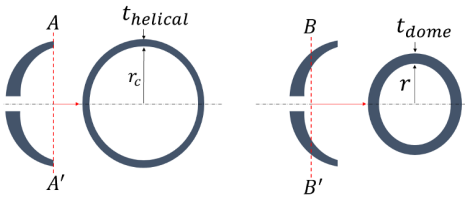

Fig. 8. Variation of composite thickness according to radius of dome in dome part.

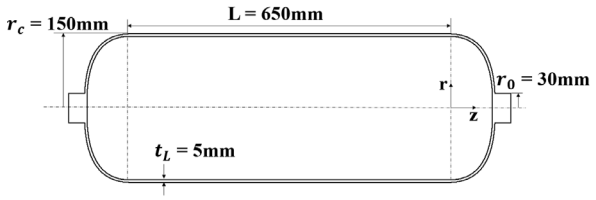

Fig. 9. Dimension of liner for pressure vessel (type 4) adopted in hydrogen automobile.

3. Design of pressure vessel (type 4) using finite element analysis

3.1 Simulation of dome part

To design liner shape of pressure vessel (type 4) as shown in Fig. 9, Isotensoid dome curve is generated using Eq. (10) when ρ_o is 0.2 (r_o = 300 mm/r_c = 150 mm), however, a combination with a spherical curve is required to remove some part of isotensoid curve because the inflection point is occurred as shown Fig. 6.

Spherical curve can be combined at an inflection point of isotensoid curve as shown in Fig. 7. When r_1 of Fig. 3 is ∞, it means $r_2 / r_1 = 0$, and the inflection point ($r_{p(I)}$) is defined by Eq. (9) as Eq. (17).

$$r_{p(I)} = \sqrt{1.5} \cdot r_o \,. \tag{17}$$

The radius (R_I), and angle (φ_p) between 'P$_I$' and z-axis on the inflection point were calculated as 382.5 mm and 6.37° by Eqs. (11) and (12), and x_0 (-289.3 mm), y_0 (0 mm) were calculated by Eqs. (13) and (15). Based on the coordinates of the inflection point calculated above, isotensoid curves combined with spherical curve at the inflection point were obtained as shown in Fig. 10.

3.2 Simulation of composite layer part

3.2.1 Calculation of thickness in the cylinder part

Thicknesses of helical and hoop layers in the cylinder part based on Eqs. (8) and (15) are 4.85 mm and 9.11 mm, respectively. Where, the longitudinal tensile strength (σ_f) of composite is 2539 MPa, and the burst pressure (P) of pressure vessel is 157.5 MPa, which is 2.25 times of working pressure (70 MPa) according to ASME Code [20]. Thickness per ply in the helical layer is 0.6 mm and that in the hoop layer is 0.3 mm, so total thicknesses of helical and hoop layers are 5.4 mm (9 plies) and 9.3 mm (31 plies), respectively, and are shown in Table 1.

Table 1. Design of composite layer for cylinder part.

Initial value		Values by calculation	
P_{burst}	157.5 Mpa	α_c	11.54°
σ_f	2539 MPa	$t_{helical}$	5.4 mm
r_c	145 mm	t_{hoop}	9.3 mm
r_o	30 mm		

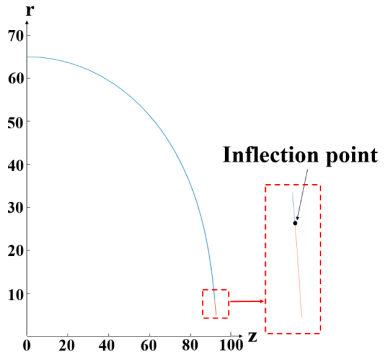

Fig. 10. Isotensoid-spherical curves combined at the inflection point (ρ_0 = 0.2).

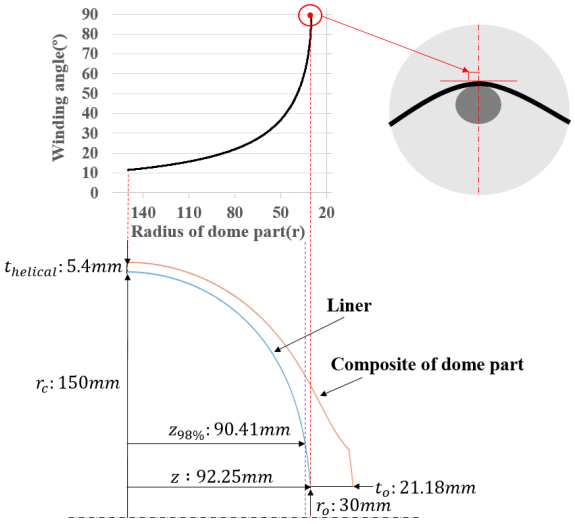

Fig. 11. The thickness according to the composite angles and radius.

3.2.2 Calculation of thickness in the dome part

Variations of thickness and laminated angle of composite layer according to dome radius (r_c : 150 mm ~ r_o : 30 mm) were calculated as shown in Fig. 11. When the dome radius is 30 mm, the laminated angle is 90° by Eq. (8), the thickness of composite by Eq. (16) is diverged at the inflection point. So the composite thickness at more than 98 % of the axial length of the dome (90.41 mm~92.25 mm) is the 21.18 mm, which is the thickness with the axial length of 90.41 mm.

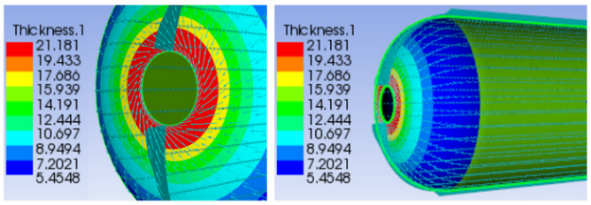

Fig. 12. 3D model of composite layer using ANSYS ACP-Pre.

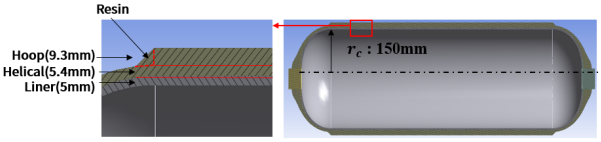

(a) Full 3D model of composite layer (hoop and helical layer)

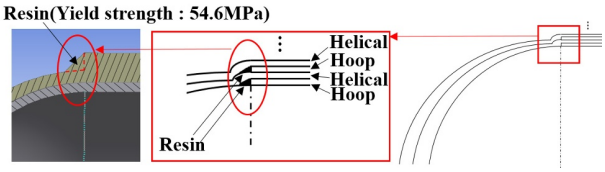

(b) Scheme of composite layer with resin

Fig. 13. Full 3D model of type 4 pressure vessel.

3.2.3 Modeling and boundary conditions

In order to verify the design method of laminated angle and thickness of composite layer calculated in Sec. 3.1, structural analysis was conducted using ANSYS workbench ver. 19.2. 3D model of the pressure vessel (type 4) was created for structure analysis. Laminated angle and thickness of composite layer was generated using ANSYS ACP-Pre as shown in Figs. 12 and 13(a) shows full model with plastic liner, aluminium boss and laminated composite layer. For in the actual field manufacturing hydrogen pressure vessel using composite, a number of helical layers and hoop layers are repeatedly stacked, and resin is filled in the empty space at the end of the hoop layer as shown in middle part of Fig. 13(b). In this study, 3D modeling of the composite layer was performed with the thicknesses (helical : 6 mm, hoop : 9.3 mm) calculated by netting analysis, and its resin (yield strength : 54.6 MPa) filled in the empty space at the end of the hoop layer during simulation was modeled as shown in left part of Fig. 13(b). Mechanical properties of composite (T700/epoxy), and aluminium alloy are shown in Table 2, where X is longitudinal direction and Y, Z and are transverse direction.

The composite and liner with aluminium boss part used 3D_8 node and 6 node structural solid element repeatedly, and a total 134900 nodes and 72182 elements were generated show Fig. 14.

The burst pressure (157.5 MPa) and the constraint conditions (fixed and displacement supports) are imposed as shown Fig. 15, and the coefficient friction was given as 0.4 between composite and liner [21].

Table 2. Material properties of composite (T700/epoxy) and aluminium 6061-T6.

Compoiste(T700/epoxy)		
Young's modulus X direction (longitudinal)	E_1 (GPa)	137
Young's modulus Y, Z direction (transverse)	$E_2 = E_3$ (GPa)	9.1
Posison's ratio XY, XZ	$\nu_{12} = \nu_{13}$	0.34
Posison's ratio YZ	ν_{23}	0.43
Shear modulus XY, XZ	$G_{12} = G_{13}$ (GPa)	4.71
Shear modulus YZ	G_{23} (GPa)	3.1
Tensile X direction	$\sigma_1 = \sigma_f$ (MPa)	2539
Aluminium 6061-T6		
Young's modulus (GPa)	71	
Poisson's ratio	0.33	
Yield strength (MPa)	280	
Tensile strength (MPa)	310	

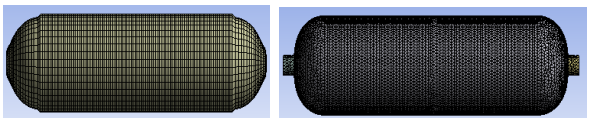

Fig. 14. Generated mesh of composite (left) and liner with boss part (right).

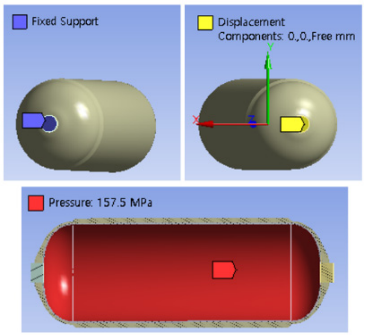

Fig. 15. Load and boundary conditions.

3.2.4 Results of simulation

The results of structural analysis regarding to inside/outside helical layer and inside hoop layer are obtained according to the axial direction of vessel. Most of loads are supported by the longitudinal tensile strength of composite. From maximum principal stresses in shown dome part of Fig. 16, they were decreasing near the boss part in case of the outside of helical layer and increasing in case of the inside of helical layer, and maximum stress occurred in the knuckle part, verified structural safety of isotensoid-spherical dome. When the burst pressure was imposed on the inner surface, maximum principal stress (σ_1) ≅ longitudinal tensile strength (σ_f) have to be satisfied. The maximum principal stresses inside hoop layer and outside helical layer were 2542.6 MPa and 2545.2 MPa, respectively, which are similar values to the longitudinal tensile strength (2539 MPa), but that inside helical layer was 2811.2 MPa in the

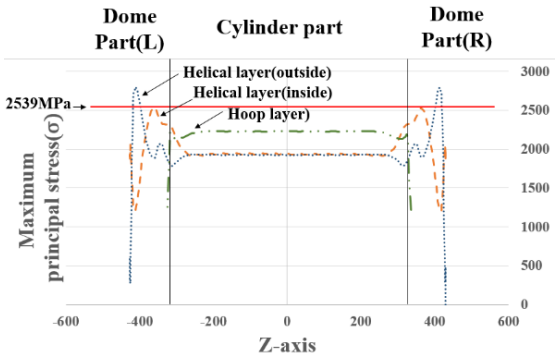

Fig. 16. Maximum principal stresses of hoop and helical composite layers according to axial direction.

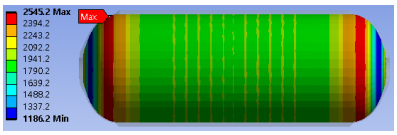

(a) Principal stress distribution of composite (inside helical layer)

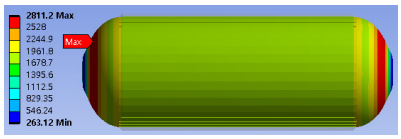

(b) Principal stress distribution of composite (outside helical layer)

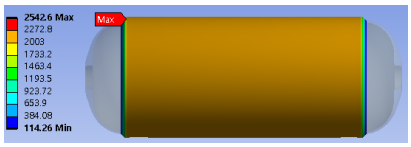

(c) Principal stress distribution of composite (hoop layer)

Fig. 17. Maximum principal stresse distribution of composite layer (helical: 5.4 mm, hoop: 9.3 mm).

dome part, which is much higher than the longitudinal tensile strength as shown in Fig. 17, so it is needed to conduct re-design of helical layer in the dome part.

When structure analysis was carried out till the thickness of helical layer was 6 mm, the maximum principal stresses are 2501.3 MPa (inside hoop layer), 2280 MPa (inside helical layer) and 2523.1 MPa (outside helical layer), and it was satisfied with the design condition ($\sigma_1 \cong \sigma_f$) as shown Fig. 18. So the optimal thicknesses of helical and hoop layers on the cylinder part were determined as 6 mm and 9.3 mm, respectively, and the composite thickness at more than 98 % of the axial length of the dome (90.41 mm~92.25 mm) is the 23.5 mm, which is the thickness with the axial length of 90.41 mm.

3.3 Optimum design of the aluminium boss

In order to achieve light-weightning and increase of inner capacity in hydrogen pressure vessel, optimal shape design of aluminium boss part was carried out using response surface

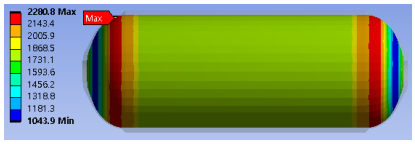

(a) Principal stress distribution of composite (inside helical layer)

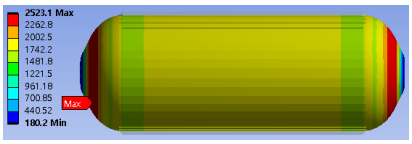

(b) Principal stress distribution of composite (outside helical layer)

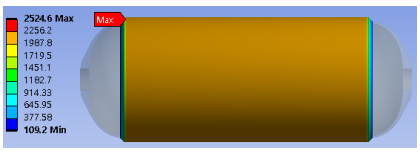

(c) Principal stress distribution of composite (hoop layer)

Fig. 18. Maximum principal stresse distribution of composite layer (helical: 6 mm, hoop: 9.3 mm).

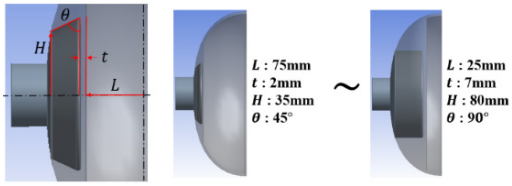

Fig. 19. Design parameter relating to boss shape.

method using ANSYS 2020 R1.

3.3.1 Determination of design parameters

Design parameters relating to the boss shape were determined as L, t, H and θ, as shown in Fig. 19, and their ranges are as follows: L_1 : 75 ~ 25 mm, t_1 : 2 ~ 7 mm, H_1 : 35 ~ 80 mm, D_1 : 45 ~ 90 ° .

The sampling points (25) were generated using OSF (optimal sapce filling) method, and the input parameters (L, H, t, θ) and the output parameters (maximum equivalent stress, mass) were set.

3.3.2 Optimal shape of boss part

Structural analyses of pressure vessels with 25 different boss model samplings were conducted. All models have the same composite shape (thickness of helical layers : 6 mm, thickness of hoop layers : 9.3 mm) suggested in Subsec. 3.2.4, and the test pressure of 105 MPa (70 MPa × 1.5) and the burst pressure of 157.5 MPa (70 MPa × 2.25) were imposed on the inner surface. Based on the above 25 case analysis, the response surface created using the genetic aggregation for optimal design of aluminium boss part, and goodness of fit was analyzed to verify quality of the response surface as shown Fig. 20. The predicted and observed chart shows the values predicted from the response surface versus the values observed

Table 3. The results of response surface optimization.

Under burst pressure (157.5 MPa)			
Al boss	Maximum equivalent stress		Tensile strength
	290.3 MPa	≤	310 MPa
Under test pressure (105 MPa)			
Al boss	Maximum equivalent stress		Yield strength
	279.9 MPa	≤	280 MPa

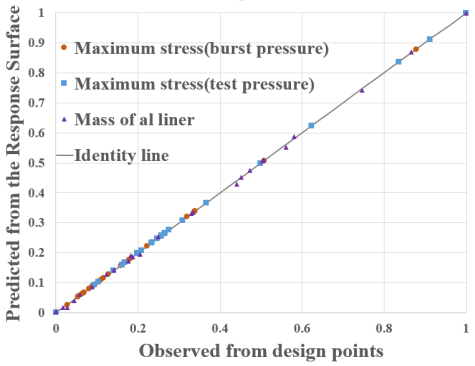

Fig. 20. Verification of response surface using goodness of fit.

from the design points. This scatter chart enables determination if the response surface correctly fits the points of the design points-table and refinement-table. The closer the points are to the diagonal line, the better the response surface fits the points. It was found that the identity line was well in agreement with the design points.

Optimization was performed to determine the optimal design of the aluminium boss part using the generated response surface, and the three requirements are as follows: maximum von-Mises stresses must be less than yield strength and tensile strength under test pressure (105 MPa) and burst pressure (157.5 MPa), respectively, and the mass (kg) of aluminium boss should be minimal. The candidate point of optimal shape (L : 67.2 mm, t : 2 mm, H: 46.6 mm θ : 88.7°) was determined through response surface, and the maximum equivalent stresses at the aluminium boss part were 290.3 Mpa (under burst pressure) and 279.9 MPa (under test pressure), respectively, which are lower than the tensile strength (310 MPa) and lower than the yield strength (280 MPa) as shown in Table 3, so it was predicted that plastic deformation does not occur in the boss shape recommend from response surface method.

To evaluate its validation, structural analysis about candidate point (L : 67.2 mm, t : 2 mm, H : 46.6 mm and θ : 88.7°) was conducted, the results are 297.7 MPa (under bust pressure) and 289.9 MPa (under test pressure) as shown in Fig. 21 which exceeded the yield strength (280 MPa) of aluminium boss, so that it is needed to re-design boss shape.

To improve the quality of the response surface for obtaining high reliability of optimal design, it is necessary to create a new

Table 4. Results of optimal design obtained from response surface method.

1st step	
Range of design parameter	L : 25 ~ 75 mm, t : 2 ~ 7 mm, H : 35 ~ 80 mm, θ : 45 ~ 90°
Candidate point predicted from response surface	L : 67.2 mm, t : 2 mm, H : 46.6 mm, θ : 88.7° σ_{max} : 290.3 MPa (burst pressure) σ_{max} : 279.9 MPa (test pressure)
Structure analysis of candidate point	σ_{max} : 297.7 MPa (burst pressure) < 310 MPa (tensile strength) σ_{max} : 289.9 Mpa (test pressure) > 280 MPa (yield strength)
State	Unsafe
2nd step	
Range of design parameter	L : 60 ~ 70 mm, t : 2 ~ 7 mm, H : 40 ~ 65 mm, θ : 70 ~ 90°
Candidate point predicted from response surface	L : 70 mm, t : 9 mm, H : 43 mm, θ : 89° σ_{max} : 290.3 MPa (burst pressure) σ_{max} : 279.9 MPa (test pressure)
Structure analysis of candidate point	σ_{max} : 334.9 MPa (burst pressure) > 310 MPa (tensile strength) σ_{max} : 285.9 Mpa (test pressure) > 280 MPa (yield strength)
State	Unsafe
3rd step	
Range of design parameter	L : 69 ~ 72 mm, t : 5 ~ 7 mm, H : 40 ~ 50 mm, θ : 89 ~ 90°
Candidate point predicted from response surface	L : 72 mm, t : 7 mm, H : 45.5 mm, θ : 89° σ_{max} : 305 MPa (burst pressure) σ_{max} : 279.9 MPa (test pressure)
Structure analysis of candidate point	σ_{max} : 306.5 MPa (burst pressure) < 310 MPa (tensile strength) σ_{max} : 279.5 Mpa (test pressure) < 280 MPa (yield strength)
State	Safe

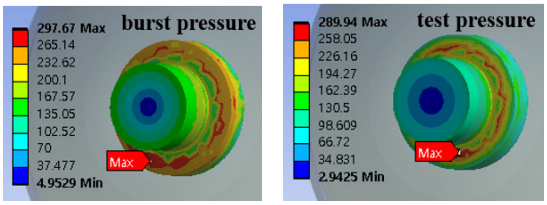

Fig. 21. Evaluation of validation of candidate point using structure analysis (1st step).

response surface with 25 design points by narrowing the ranges of the design parameters based on the first optimal model. The optimal boss shape to satisfy design conditions (yield strength 280 MPa, tensile strength 310 MPa) was obtained through 3 times above procedures repeatedly, and the results were shown in Table 4.

Aluminium boss shape obtained from candidate points was shown Fig. 22, and results of its structural analysis were 306.5 MPa (under burst pressure) and 279.5 MPa (under test pressure) as shown in Fig. 23.

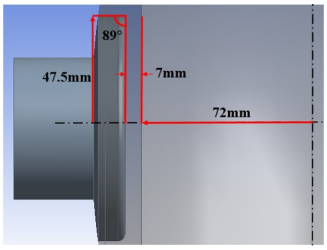

Fig. 22. Dimension of aluminium boss part from obtained response surface method.

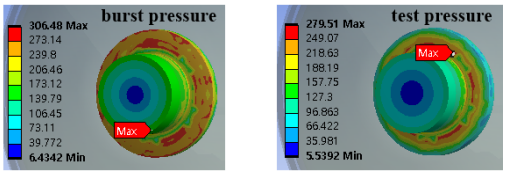

Fig. 23. Evaluation of validation of candidate point using structure analysis (3rd step).

(a) Principal stress distribution of composite (inside helical layer)

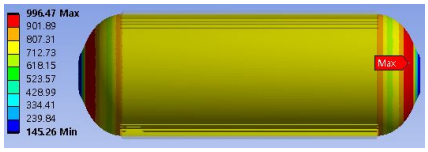

(b) Principal stress distribution of composite (helical outside layer)

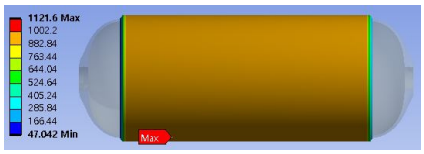

(c) Principal stress distribution of composite (hoop layer)

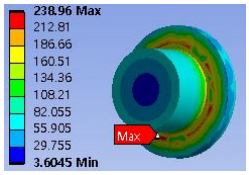

(d) Equivalent stress distribution of aluminium boss

Fig. 24. Stress distribution of the optimal model under the working pressure (70 MPa).

3.4 Structural safety verification of the optimal model

Structure analysis of the optimal pressure vessel with composite layer (helical : 6 mm, hoop : 9.3 mm) and the boss part (L : 72 mm, t : 7 mm, H : 47.5 mm, θ : 89°) was conducted under the working pressure (70 MPa), and the stress distributions are shown in Fig. 24. The maximum principal stresses occuring at the composite are 1095 MPa (inside helical), 996.5 MPa (outside helical) and 1121.6 MPa (inside hoop), respectively, which are little lower than the longitudinal tensile strength (2539 MPa), and the maximum equivalent stress occuring at the boss is 239 MPa, which is lower than the yield strength (280 MPa), as shown in Table 5, so that structural safety of the optimal model was verified.

Table 5. Resutls of structure analysis of type 4 pressure vessel under working pressure (70 MPa).

Helical layer (inside)	Maximum principal stress (σ_1)		Longitudinal tensile strength (σ_f) (2539 MPa)
	1095 MPa	≤	
Helical layer (outside)	Maximum principal stress (σ_1)		
	996.4 MPa	≤	
Hoop layer	Maximum principal stress (σ_1)		
	1121.6 MPa	≤	
Al boss	Maximum von-Mises stress		Yield strength
	239 MPa	≤	280 MPa

4. Conclusions

This study has carried out to obtain structural safety of hydrogen pressure vessel (type 4) under working pressure (70 MPa). The results of the study were summarized as follows.

1) Isotensoid-spherical dome was designed for filament wound without slip, and thicknesses of composite layer to satisfy structural safety were determined as follows.

- Cylinder part: Helical and hoop thickness = 6 mm, 9.3 mm.
- Dome part: Helical thickness = 23.5 mm.

2) Maximum principal stresses occurring at the composite were decreasing near the boss part in case of the outside of helical layer and increasing in case of the inside of helical layer and occurred in the knuckle part, which was seem to be similar trend of vessel and verified structural safety of isotensoid-spherical dome.

3) The shape of aluminium boss obtained using response surface method 3 times to improve the quailty of it was as follows:

- Optimal shape: L = 72 mm, t = 7 mm, H = 47.5 mm, θ = 89°.

4) Safety of the hydrogen pressure vessel with the optimal shape of boss part obtained from response surface method and the optimal thicknesses of composite layer by FEM was verified under working pressure (70 MPa).

Acknowledgments

This work was supported by National Research Foundation of Korea (NRF) grant funded by the Korea government (MSIT)

(No. 2019R1F1A1058521).

Nomenclature

r_1 : Meridian curvature radius
r_2 : Circumferential curvature radius
r_o : Ridius of boss
r_c : Ridius of cylinder
N_θ : Circumferential line load
N_φ : Meridian line load
σ_f : Longitudinal tensile strength of composite
σ_1 : Maximum principal stress
σ_{max} : Maximum equivalent stress
t : Thickness of helical layer on the dome part
t_{hoop} : Thickness of hoop layer on the cylinder part
$t_{helical}$: Thickness of helical layer on the dome part
α : Laminated angle of helical layer on the dome part
α_c : Laminated angle of helical layer on the cylinder
P : Internal pressure

References

[1] N. L. Panwar, S. C. Kaushik and S. Kothari, Role of renewable energy sources in environmental protection: a review, *Renewable and Sustainable Energy Reviews*, 15 (2011) 1513-1524.
[2] J. Gangloff, J. Kast, G. Morrison and J. Marcinkoski, Design space assessment of hydrogen storage onboard medium and heavy duty fuel cell electric trucks, *Journal of Electrochemical Energy Conversion and Storage*, 14/021004-1 (2017).
[3] H. Barthelemy, M. Weber and F. Barbier, Hydrogen storage: recent improvements and industrial perspectives, *International Journal of Hydrogen Energy*, 42 (2017) 7254-7262.
[4] J. Humberto, S. Almeida, H. Faria, T. Marques and C. Amico, Load sharing ability of the liner in type III composite pressure vessels under internal pressure, *Journal of Reinforced Plastics & Composites*, 33 (24) (2014) 2274-2286.
[5] J. P. B. Ramirez, D. Halm and J. C. Grandidier, 700 bar type IV high pressure hydrogen storage vessel burst - simulation and experimental validation, *International Journal of Hydrogen Energy*, 40 (2015) 13183-13192.
[6] F. Hayato, Y. Akinori and M. Ryosuke, Structural optimization for cryogenic tank based on energy release rate, *Composte Structures*, 152 (2016) 883-890.
[7] S. M. Cho, K. S. Kim, S. K. Lee, G. S. Jung, S. K. Lee and S. K. Lyu, Effect of dome curvature on failure mode of type 4 composite pressure vessel, *International Journal of Precision Engineering And Manufacturing,* 19 (3) (2018) 405-410.
[8] V. Alcantar, S. M. Aceves, E. Ledesma, S. Ledesma and E. Aguilera, Optimization of type 4 composite pressure vessels using genetic algorithms and simulated annealing, *International Journal of Hydrogen Energy,* 42 (2017) 15770-15781.
[9] H. S. Roh, T. Q. Hua and R. K. Ahluwalia, Optimization of carbon fiber usage in type 4 hydrogen storage tanks for fuel cell automobiles, *International Journal of Hydroen Energy*, 38 (2013) 12795-12802.
[10] T. Q. Hua, H. S. Roh and R. K. Ahluwalia, Performance assessment of 700-bar compressed hydrogen storage for light duty fuel cell vehicles, *International Journal of Hydrogen Energy,* 42 (2017) 25121-25129.
[11] D. Leh, P. Saffre, P. Francescato, R. Arrieux and S. Villalonga, A progressive failure analysis of a 700-bar type IV hydrogen composite pressure vessel, *International Journal of Hydrogen Energy,* 40 (2015) 13206-13214.
[12] Z. Lei, K. Sotiris and B. Adriaan, Design of filament-wound isotensoid pressure vessels with unequal polar openings, *Composite Structures*, 92 (2010) 2307-2313.
[13] E. S. Barboza, M. Chludzinski, P. B. Roese, J. S. O. Fonseca, S. C. Amico and C. A. Ferreira, Experimental and numerical analysis of a LLDPE/HDPE liner for a composite pressure vessel, *Polymer Testing*, 30 (2011) 693-700.
[14] Z. Lei, K. Sotiris and B. Adriaan, Design of filament-wound domes based on continuum theory and non-geodesic roving trajectories, *Composite: Part A*, 41 (2010) 1312-1320.
[15] S. M. Cho, K. S. Kwang, K. M. Lee, S. K. Lee, Y. J. Lee and S. K. Lyu, A study on cycling life and failure mode of type 3 cylinder treated with autofrettage pressure, *Interantion Journal of Precision Engineering and Manufacturing,* 17 (12) (2016) 1685-1691.
[16] Z. Kabir, Finite element analysis of composite pressure vessels with a load sharing metallic liner, *Composite Structures*, 49 (2000) 247-255.
[17] M. D. Musthak, P. Madar and S. Narayana, Prediction of transverse directional strains and stresses of filament woun composite pressure vessel by using higher order shear deformation theories, *International Journal of Composite Materials*, 6 (3) (2016) 79-87.
[18] R. P. Nair and R. Kumar, A new concept in the design for filament wound composite pressure vessel, *International Journal of Engineering Research and Science & Technology*, 3 (1) (2016) 208-213.
[19] C. U. Kim, J. H. Kang, C. S. Hong and C. G. Kim, Optimal design of filament wound structures under internal pressure based on the semi-geodesic path algorithm, *Composite Structures*, 6792005 (2016) 443-452.
[20] ASME, *BPVC Section X - Fiber-reinforced Plastic Pressure Vessels*, The American Society of Mechanical Engineers, New York City (2019).
[21] M. G. Han and S. H. Chang, Failure analysis of a type III hydrogen pressure vessel under impact loading induced by free fall, *Composite Structures*, 127 (2015) 288-297.

Gunyoung Park is in a Doctor's course in the School of Mechanical Engineering, Pusan National University, Busan, Korea. He received Master's degree of Mechanical Convergence Technology at Pusan National University in 2018. His major research fields are metal forming, design of composite and pressure vessel.

Hyoseong Jang is in a Doctor's course in the School of Mechanical Engineering, Pusan National University, Busan, Korea. He received Master's degree of Creative Engineering System at Pusan National University in 2015. His major research fields are gear design and computational fluid dynamics.

Chul Kim is a Professor of Mechanical Engineering at Pusan National University, Korea. He received doctoral degree of Mechanical Engineering at Pusan National University in 2011. His major research fields extend into FEM simulation (structure, dynamic and fluid analysis), optimal structural design, CAD/CAM.